

Short note

Asymmetric push-pull small molecules with auxiliary electron-accepting unit for bulk heterojunction organic solar cells

Ying Chen^a, Duo Yang^b, Wei Liu^c, Junfeng Tong^a, Chunyan Yang^a, Peng Zhang^{a,*}^a School of Materials Science and Engineering, Lanzhou Jiaotong University, Lanzhou, 730070, China^b Key Laboratory of Optoelectronic Technology and Intelligent Control of Ministry Education, Lanzhou Jiaotong University, Lanzhou, 730070, China^c Key Laboratory of Nonferrous Metals Chemistry and Resources Utilization of Gansu Province, State Key Laboratory of Applied Organic Chemistry and College of Chemistry and Chemical Engineering, Lanzhou University, Lanzhou, 730000, China

ARTICLE INFO

Keywords:

Small molecular donor
Asymmetrical push-pull
Donor-acceptor-acceptor
Photovoltaic properties

ABSTRACT

Two small molecular donors (TPA-DPP and TPA-DPP-MDN) were designed with asymmetric push-pull structure, namely, donor-acceptor (D-A) and donor-acceptor-acceptor (D-A-A) systems. They were synthesized and investigated by thermogravimetric analysis, UV-vis spectra, X-ray diffraction, density functional theory (DFT) calculation, electrochemical and the photovoltaic (PV) measurement. The D-A-A architecture (TPA-DPP-MDN) exhibited lower highest occupied molecular orbital (HOMO) of -5.18 eV, narrower optical band gap of 1.52 eV, better thermal stability and higher degree of ordered aggregation than these of the D-A system (TPA-DPP). TPA-DPP-MDN based PV device showed better performance with higher open-circuit voltage (V_{OC}) and short-circuit current density (J_{SC}) than these of TPA-DPP based PV devices due to the low-lying HOMO level and wide spectral absorption range of TPA-DPP-MDN.

1. Introduction

The organic solar cells (OSCs) based on small molecular donors (SMDs) have benefit gained immense interests due to constantly increased efficiencies [1–3], and the uniqueness over conventional polymers such as structural adjustability, high purity, batch-to-batch reproducibility, and so on [4,5]. Among small molecular donors, SMDs with push-pull systems have drawn more and more attention [6–9]. These SMDs featured donor-acceptor (D-A) configuration typically, demonstrated an important advantage in molecular design flexibility, which allowed for fine and precise tuning of the photophysical properties, such as frontier orbital level alignment, band gap (E_g), and light-absorption ability [10–12].

In general, the SMDs with promising photovoltaic (PV) performance based on the symmetrical D-A-D and A-D-A structures have been developed [6,8,13–17]. In contrast, the PV properties of the asymmetric push-pull SMDs have lagged far behind these of the symmetrical system-based OSCs [18–21]. Recently, Wong et al and Yin et al have developed a novel asymmetric push-pull system in which an auxiliary electron-withdrawing unit was introduced into the D-A structure to propose a D-A-A structure [22–25]. These SMDs realized the high PV performance possessing extended spectral regions by reducing the band gap (E_g) in compared with the SMDs featured D-A structure

[18,22]. Furthermore, theoretical research suggested several favourable characteristics of the D-A-A structure as following [26,27]: (i) enhancing the intramolecular charge transfer; (ii) modulating the energy gap and the response of the light-harvesting range expediently; Interestingly, the SMDs with D-A-A structure may become a reliable route for designing organic absorber toward highly efficient SMDs. However, the SMDs based on D-A-A systems have been relatively less explored and studied [23,25]. And thus, it was necessary to pursue the objective of understanding the structure-property relationships in this class of molecules (D-A-A system) to provide an insight into the molecular design of asymmetric push-pull SMDs.

In this paper, two asymmetric push-pull molecules (TPA-DPP-MDN and TPA-DPP) have been designed and synthesized, as shown in Scheme 1. Specifically, these molecules were designed with the following structural characteristics: (i) the TPA-DPP with D-A structure was consisting of phenyl-di-*p*-tolyl-amine (TPA) moiety as a D unit and diketopyrrolopyrrole (DPP) as a A group; (ii) the 2-benzylidene-malononitrile (MDN) group as auxiliary electron-withdrawing unit was introduced into the molecule to form D-A-A structure. In compare with TPA-DPP, the TPA-DPP-MDN showed an extended spectral region with a E_g of 1.52 eV and relatively low-lying lower highest occupied molecular orbital (HOMO) energy level. Furthermore, TPA-DPP-MDN possessed higher degree of crystallinity than TPA-DPP in pristine film

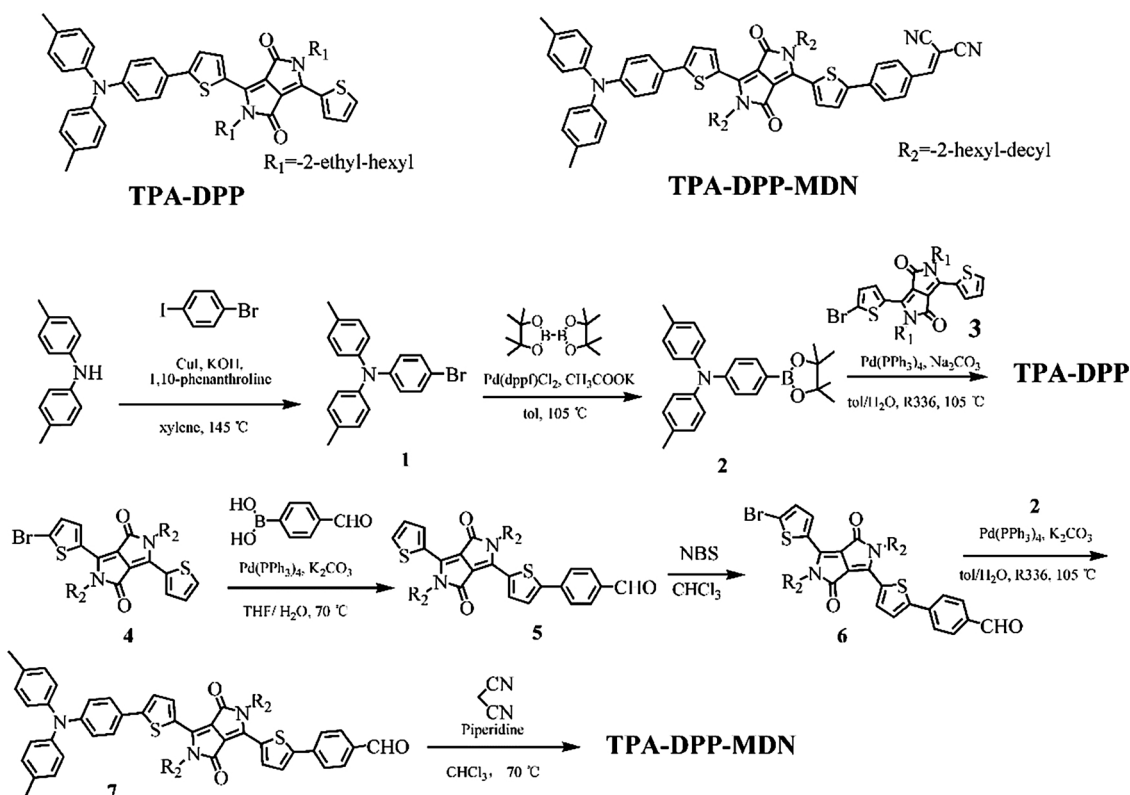
* Corresponding author.

E-mail address: xiaozhangfei.feizhang@163.com (P. Zhang).<https://doi.org/10.1016/j.jphotochem.2019.112139>

Received 13 June 2019; Received in revised form 10 September 2019; Accepted 2 October 2019

Available online 04 October 2019

1010-6030/© 2019 Published by Elsevier B.V.



Scheme 1. Molecular structure and Synthetic route of TPA-DPP and TPA-DPP-MDN.

according to the XRD data. Their PV properties were investigated, employing these molecules as the electron donor and PC₆₁BM as the electron acceptor. The results showed that the D-A-A based device gave a significantly improved performance with enhanced open-circuit voltage (V_{OC}) and short-circuit current density (J_{SC}). This encouraging result indicated a great potential of such D-A-A systems in developing high-performance SMD materials.

2. Experimental

2.1. Materials and general methods

All reagents were purchased from Aldrich, Acros, and TCI Chemical Co. The solvents were further purified under nitrogen flow. Compound 3 and 4 were prepared according to reference [28]. The ¹H NMR spectra were attained on a Bruker DRX 400 spectrometer at 400 MHz. Elemental analysis was performed on a Vario EL elemental analysis instrument. The high-resolution mass spectra (HRMS) of TPA-DPP and TPA-DPP-MDN were collected using Thermo Scientific Q Exactive. The thermal stability of the material was achieved using thermal gravimetric analysis (TGA) 2050 with a heating rate of 10 °C min⁻¹ and a range of 25 °C to 600 °C under nitrogen. The UV-vis absorption spectra were carried out by Shimadzu UV-1800 spectrometer. The fluorescence spectra of TPA-DPP (a) and TPA-DPP-MDN (b) in different solvents have been measured on 970CRT fluorescence spectrophotometer. CHI 600D electrochemical workstation was employed for cyclic voltammetry (CV) measurements using a three-electrode cell of which equipped with a Pt wire counter electrode, a glass carbon working electrode and an Ag/AgNO₃ reference electrode standardized with the internal standard of ferrocene. The CV measurements were performed at an electrolyte with 0.1 M tetrabutylammonium hexafluorophosphate in anhydrous nitrogen-saturated acetonitrile with a scan rate 100 mV s⁻¹. The X-ray diffraction (XRD) was accomplished on a PANalytical X'Pert PRO diffractometer (Cu K α radiation, $\lambda = 1.54 \text{ \AA}$).

2.2. Synthesis

2.2.1. Synthesis of compound 1

4,4'-Dimethyldiphenylamine (5 g, 14.2 mmol), 1-bromo-4-iodobenzene (7.90 g, 27.9 mmol), CuI (2.40 g, 12.6 mmol), KOH (6.93 g, 123 mmol) and 1,10-phenanthroline (1.3 g, 6.57 mmol) in anhydrous (30 mL) xylene and then the solution was refluxed under argon for 20 h at the temperature of 145 °C. After being cooled to the room temperature, the mixture was poured into 300 mL water and the organic layer was separated. The aqueous layer was extracted with CH₂Cl₂ (3 × 40 mL) and the combined organic layers were dried over anhydrous Na₂SO₄. A white solid 1 (4.70 g) was obtained via column chromatography (silica gel 200–300 mesh) using petroleum ether by volume as eluent. Yield: 52.6%. ¹H NMR (400 MHz, CDCl₃), δ (ppm): 7.26 (d, $J = 8.0$ Hz, 2 H), 7.06 (d, $J = 8.0$ Hz, 2 H), 6.96 (d, $J = 8.0$ Hz, 4 H), 6.87 (d, $J = 8.0$ Hz, 4 H), 2.30 (s, 6 H).

2.2.2. Synthesis of compound 2

Bromide 1 (2 g, 5.68 mmol), bis(pinacolato)diboron (3.12 g, 12.3 mmol), Pd(dppf)Cl₂ (70 mg), CH₃COOK (2.4 g, 24.5 mmol), then the mixture of toluene (20 mL) added into the two-neck flask and was refluxed for 12 h at the temperature of 105 °C under argon. After being cooled to the room temperature, the mixture was poured into 300 mL water and the organic layer was separated. The aqueous layer was extracted with CH₂Cl₂ (3 × 40 mL) and the combined organic layers were dried over anhydrous Na₂SO₄. The organic solvent was evaporated, and the crude product was purified via column chromatography (silica gel 200–300 mesh) using petroleum ether by volume as the eluent to afford milky solid 3 (1.57 g), Yield: 58%. ¹H NMR (400 MHz, CDCl₃), δ (ppm): 7.62 (d, $J = 8.0$ Hz, 2 H), 7.07 (d, $J = 8.0$ Hz, 4 H), 7.00 (d, $J = 8.0$ Hz, 4 H), 6.96 (d, $J = 8.0$ Hz, 2 H), 2.31 (m, 6 H), 1.32 (m, 12 H).

2.2.3. Synthesis of compound 5

Compound 4 (2 g, 2.42 mmol), 4-Formylphenylboronic acid (1.30 g, 8.66 mmol), by using Pd(PPh₃)₄ (200 mg), K₂CO₃ (3.50 mg, 25.4 mmol)

as catalyst, then the THF (50 mL), H₂O (5 mL), R336 (5 drops) added into the two-neck flask and was refluxed for 15 h at the temperature of 70 °C under argon. After being cooled to the room temperature, the mixture was poured into 300 mL water and the organic layer was separated. The aqueous layer was extracted with CH₂Cl₂ (3 × 40 mL) and the combined organic layers were dried over anhydrous Na₂SO₄ and the organic solvent was removed under reduced pressure. A purple solid **5** (1.70 g) was obtained via column chromatography (silica gel 200–300 mesh) using ethyl acetate:petroleum ether = 1:10 by volume as eluent. Yield: 75.6%. ¹H NMR (400 MHz, CDCl₃), δ (ppm): 10.04 (s, 1 H), 8.92 (d, J = 4.0 Hz, 1 H), 8.90 (d, J = 4.0 Hz, 1 H), 7.94 (d, J = 8.0 Hz, 2 H), 7.83 (d, J = 8.0 Hz, 2 H), 7.65 (d, J = 8.0 Hz, 1 H), 7.60 (d, J = 4.0 Hz, 1 H), 7.28 (t, J = 12.0 Hz, 1 H), 4.07–4.03 (m, 4 H), 1.95–1.91 (m, 2 H), 1.33–1.22 (m, 48 H), 0.87–0.82 (m, 12 H).

2.2.4. Synthesis of compound 6

Compound **5** (1.50 g, 1.61 mmol) was dissolved in 40 mL CHCl₃ and a solution of NBS (300 mg, 1.69 mmol) in 30 mL CHCl₃ was added dropwise to the solution. Then the mixture was stirred under at room temperature without light for 15 h. The organic solvent was evaporated, and the crude product was purified via column chromatography (silica gel 200–300 mesh) using ethyl acetate:petroleum ether = 1:10 by volume as the eluent to afford solid **6** (0.940 g), Yield: 57.5%. ¹H NMR (400 MHz, CDCl₃), δ (ppm): 10.04 (s, 1 H), 8.91 (d, J = 4.0 Hz, 1 H), 8.66 (d, J = 4.0 Hz, 1 H), 7.94 (d, J = 8.0 Hz, 2 H), 7.83 (d, J = 8.0 Hz, 2 H), 7.60 (d, J = 4.0 Hz, 1 H), 7.23 (d, J = 8.0 Hz, 1 H), 4.05 (d, J = 8.0 Hz, 2 H), 3.95 (d, J = 8.0 Hz, 2 H), 1.95–1.91 (m, 2 H), 1.31–1.23 (m, 48 H), 0.87–0.80 (m, 12 H).

2.2.5. Synthesis of compound 7

Compound **2** (400 mg, 0.396 mmol), compound **6** (200 mg, 0.501 mmol), using Pd(PPh₃)₄ (25 mg), Na₂CO₃ (110 mg, 1.04 mmol), the toluene (20 mL), H₂O (2 mL), R336 (2 drops) as catalyst then the solution was refluxed Suzuki coupling for 12 h under argon atmosphere at the temperature of 105 °C. After being cooled to the room temperature, the solution was poured into 100 mL water and extracted with CH₂Cl₂ (3 × 20 mL). The combined organic layers were dried over anhydrous Na₂SO₄ and the organic solvent was removed under reduced pressure. A solid **7** (300 mg) was obtained via column chromatography (silica gel 200–300 mesh) using petroleum ether by volume as eluent. Yield: 62.9%. ¹H NMR (400 MHz, CDCl₃), δ (ppm): 10.06 (s, 1 H), 9.05 (d, J = 8.0 Hz, 1 H), 8.87 (d, J = 4.0 Hz, 1 H), 7.93 (d, J = 8.0 Hz, 2 H), 7.83 (d, J = 8.0 Hz, 2 H), 7.59 (d, J = 4.0 Hz, 1 H), 7.49 (d, J = 8.0 Hz, 2 H), 7.36 (d, J = 4.0 Hz, 1 H), 7.11 (d, J = 8.0 Hz, 4 H), 7.05–6.99 (m, 6 H), 4.07 (t, J = 12.0 Hz, 4 H), 2.34 (s, 6 H), 2.03–1.94 (m, 2 H), 1.34–1.22 (m, 48 H), 0.85–0.79 (m, 12 H).

2.2.6. Synthesis of TPA-DPP

Borate ester **2** (150 mg, 0.376 mmol), bromide **3** (140 mg, 0.196 mmol) using Pd(PPh₃)₄ (20 mg), Na₂CO₃ (106 mg, 1.00 mmol) as catalyst, then the toluene (7 mL), H₂O (1 mL), R336 (2 drops) added into the 25 mL two-neck flask and was refluxed for 5 h at the temperature of 105 °C under argon. After being cooled to the room temperature, the solution was poured into 100 mL water and extracted with CH₂Cl₂ (3 × 20 mL). The combined organic layers were dried over anhydrous Na₂SO₄. The organic solvent was evaporated, and the crude product was purified via column chromatography (silica gel 200–300 mesh) using dichloromethane:petroleum ether = 1.5:1 by volume as the eluent to afford purple black solid. Then, the solid was dissolved with trichloromethane, which was poured into methanol. The precipitate was collected and dried under vacuum over night (yield: 65%). ¹H NMR (400 MHz, CDCl₃), δ (ppm): 9.02 (d, J = 4.0 Hz, 1 H), 8.86 (d, J = 4.0 Hz, 1 H), 7.60 (d, J = 4.0 Hz, 1 H), 7.49 (d, J = 8.0 Hz, 2 H), 7.35 (d, J = 4.0 Hz, 1 H), 7.27 (t, J = 12.0 Hz, 1 H), 7.11 (d, J = 8.0 Hz, 4 H), 7.05–7.00 (m, 6 H), 4.04 (t, J = 12.0 Hz, 4 H), 2.34 (s, 6 H), 1.94–1.87 (m, 2 H), 1.40–1.26 (m, 16 H), 0.92–0.84 (m, 12 H). ¹³C NMR

(600 MHz, CDCl₃) δ (ppm): 161.91, 161.54, 150.52, 149.00, 144.51, 140.75, 139.16, 137.52, 134.77, 133.47, 130.05, 130.02, 130.00, 128.32, 127.33, 126.82, 125.53, 125.22, 123.16, 121.46, 108.21, 107.47, 45.91, 45.87, 39.18, 39.08, 31.91, 30.90, 30.23, 29.68, 29.64, 29.34, 28.47, 28.36, 23.65, 23.55, 23.07, 23.05, 22.68, 20.86, 14.10, 14.04, 14.01, 10.56, 10.50. TPA-DPP HRMS: 795.3879 [M⁺] (calcd for C₅₀H₅₇O₂N₃S₂: 795.3887). Anal. Calcd for C₅₀H₅₇N₃O₂S₂: C, 75.43; H, 7.22; N, 5.28; Found: C, 75.49; H, 7.31; N, 5.22.

2.2.7. Synthesis of compound TPA-DPP-MDN

Compound **7** (150 mg, 0.125 mmol), malononitrile (13 mg, 0.188 mmol), piperidine (2 drops), then the CHCl₃ (7 mL) added into the 25 mL two-neck flask and was refluxed for 7 h at the temperature of 65 °C under argon. After being cooled to the room temperature, the solution was poured into 100 mL water and extracted with CH₂Cl₂ (3 × 20 mL). The combined organic layers were dried over anhydrous Na₂SO₄. The organic solvent was evaporated, and the crude product was purified via column chromatography (silica gel 200–300 mesh) using dichloromethane:petroleum ether = 3:1 by volume as the eluent to afford purple black solid. Then, the solid was dissolved with trichloromethane, which was poured into methanol. The precipitate was collected and dried under vacuum over night (yield: 57.5%). ¹H NMR (400 MHz, CDCl₃), δ (ppm): 9.08 (d, J = 4.0 Hz, 1 H), 8.87 (d, J = 4.0 Hz, 1 H), 7.96 (d, J = 8.0 Hz, 2 H), 7.81 (d, J = 8.0 Hz, 2 H), 7.72 (s, 1 H), 7.61 (d, J = 8.0 Hz, 1 H), 7.49 (d, J = 8.0 Hz, 2 H), 7.37 (d, J = 4.0 Hz, 1 H), 7.11 (d, J = 8.0 Hz, 4 H), 7.05–6.99 (m, 6 H), 4.07–4.04 (m, 4 H), 2.34 (s, 6 H), 2.03–1.94 (m, 2 H), 1.34–1.22 (m, 48 H), 0.85–0.79 (m, 12 H). ¹³C NMR (400 MHz, CDCl₃) δ (ppm): 161.86, 161.28, 158.09, 151.32, 149.19, 145.59, 144.39, 141.44, 138.95, 138.25, 137.51, 135.84, 133.62, 131.59, 130.41, 130.07, 127.05, 126.83, 126.63, 125.31, 125.20, 123.18, 121.21, 113.83, 112.75, 109.48, 107.58, 81.96, 46.33, 37.95, 37.88, 31.83, 31.80, 31.27, 30.91, 30.02, 29.71, 29.68, 29.54, 29.27, 26.30, 22.60, 20.87, 14.08. TPA-DPP-MDN HRMS: 1171.6762 [M⁺] (calcd for C₇₆H₉₃O₂N₅S₂: 1171.6765). Anal. Calcd for C₇₆H₉₃N₅O₂S₂: C, 77.84; H, 7.99; N, 5.97; Found: C, 77.88 H, 7.93; N, 5.94.

2.3. Photovoltaic cells devices fabrication and characterization

Prior to use, a patterned indium tin oxide (ITO) glass substrate with a resistance of 10–15 Ω/square were rinsed with ultrasonication in deionized water, acetone and i-propanol, sequentially. The inverted devices were fabricated with the configuration ITO/PFN/SMDs:PC₆₁BM/MoO₃/Ag. The PFN was dissolved in methanol with tiny amounts of acetic acid to prepare 1 mg mL⁻¹ solution. Then the PFN solution were spun on the cleaned ITO substrate. The thickness (10 nm-thick) of the interlayer was monitored by a surface Tencor Alpha-500 profilometer. The active layer (60–70 nm) films of TPA-DPP (or TPA-DPP-MDN)/PC₆₁BM (1:3 Wt. ratio) were prepared by the spin-coating method on the top of interlayer in chloroform solution, respectively. After drying the solvent, a mask was attached, and the MoO₃ (8 nm) and Ag (80 nm) layer were deposited by thermal evaporation under a pressure of 5 × 10⁻⁴ Pa, successively. The effective area of device was defined by masks about 0.10 cm². The thickness of the MoO₃ and Ag was recorded by a Shenyang Sciens quartz SI-TM206 crystal thickness/ratio monitor. All the fabrication steps were performed in a Etelux glove box filled with high-purity nitrogen. The PCEs of the PSCs were measured using a San-EI Electric XEC-300M2 solar simulator, under a sun AM 1.5 G irradiation with the intensity of 100 mW·cm⁻². The current density-voltage (*J*-*V*) characteristics were carried out using a Keithley 2400 source-measurement unit. Incident photon to charge carrier efficiency (IPCE) of the devices were characterized by a Beijing 7-star Opt 7-SCSpecIII commercial incident photon. A calibrated silicon detector was used to determine the absolute photo sensitivity.

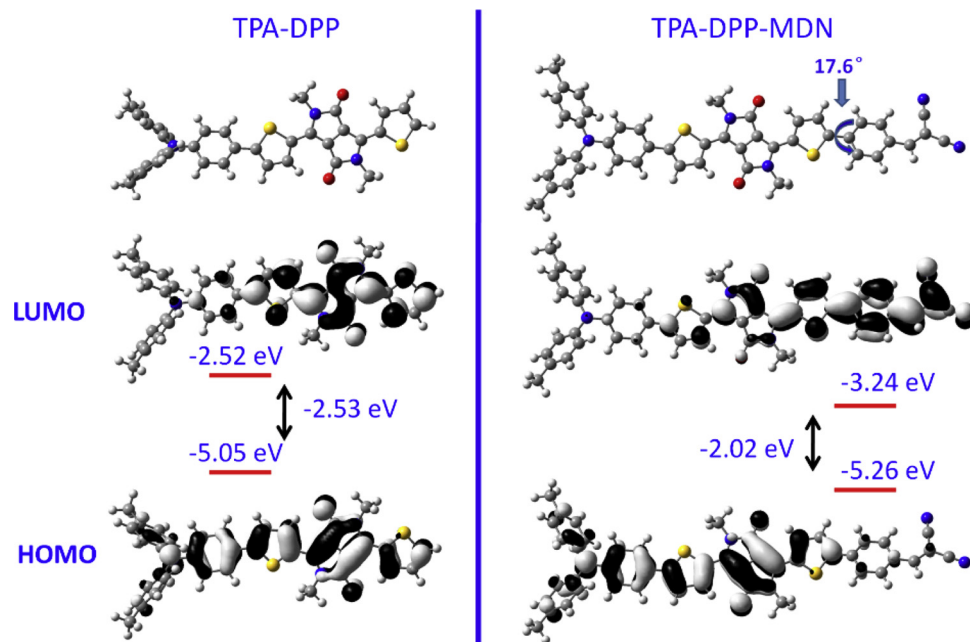


Fig. 1. Optimized geometries and surface plots of TPA-DPP and TPA-DPP-MDN by DFT at the PBE0/6-311G*.

3. Results and discussion

3.1. Theoretical calculations

Calculations were carried on the two small molecules by using density functional theory (DFT) calculation with PBE0/6-311G* basis set, as implemented in Gaussian 09 [29]. To simplify the calculation, the side alkyl chains were modified to methyl groups. The calculated energy levels and electronic-density distribution were shown in Fig. 1. The computational analysis showed that the dihedral angle of the thiophene and MDN linked around the single bond was 17.6° , which presented a near coplanar conformations. The MDN moiety not only extended electronic conjugation across successive aromatic segments along the conjugated backbone, but also led to an increase in facilitating the intramolecular charge transfer (ICT) from donor group to the acceptors. Fig. 1 showed the molecular orbital distributions of HOMO and lowest unoccupied molecular orbital (LUMO) isosurfaces of two models. The HOMO orbital distribution for TPA-DPP was equally distributed the whole conjugated backbones, while the LUMO was significantly localized on the electron accepting moieties. In the case of D-A-A system, the HOMO was distributed on the donor and DPP group, whereas LUMO was located on the acceptors, mainly in MDN moiety, indicating an apparent ICT characteristic. In addition, the calculation results gave the HOMO/LUMO levels of $-5.05/-2.52$ eV for TPA-DPP and $-5.26/-3.24$ eV for TPA-DPP-MDN, corresponding to energy gaps (E_g) of 2.53 eV for TPA-DPP and 2.02 eV for TPA-DPP-MDN. Compared with the TPA-DPP, the TPA-DPP-MDN exhibited a decrease in both the HOMO and LUMO energy levels. Moreover, the LUMO level was lowered by a larger amount than the HOMO level. The increased E_g^{opt} for D-A system may indicate that the low-energy absorption band dominated by HOMO to LUMO transition of TPA-DPP was blue-shifted compared to that of TPA-DPP-MDN.

3.2. Thermal properties

Thermal stabilities of the small molecules were important for the fabrication process of the photovoltaic device. Their thermal stabilities were studied by thermogravimetric-analysis (TGA), which was shown in Fig. 2. The temperatures at 5% weight loss were selected as onset point of decompositions. Both the SMDs exhibited high thermal

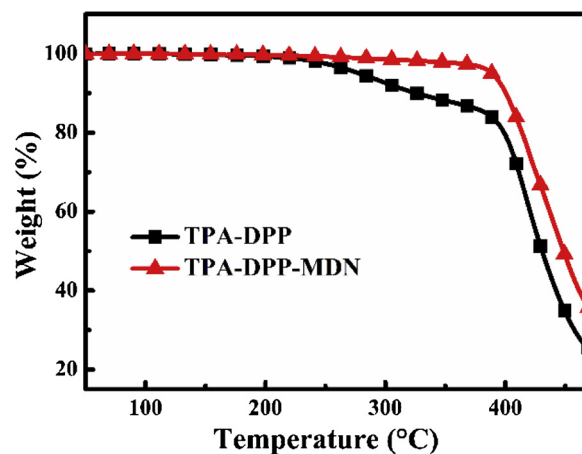


Fig. 2. TGA plots at a heating rate of $10^\circ\text{C min}^{-1}$ under a nitrogen atmosphere of TPA-DPP and TPA-DPP-MDN.

stability, the onset decompositions of TPA-DPP and TPA-DPP-MDN were 275°C and 388°C , respectively. Obviously, TPA-DPP-MDN has a better thermal stability for long-term applications with respect to TPA-DPP.

3.3. X-ray diffraction

X-ray diffraction (XRD) was performed to investigate the aggregation ordered structures of the TPA-DPP and TPA-DPP-MDN in the pristine films. Fig. 3 showed the XRD patterns of the corresponding films. The XRD pattern of TPA-DPP-MDN featured a relatively sharp peak at 2θ of 5.56° with a d -spacing of 15.71 \AA , which revealed a high degree of crystallinity and a lamellar structure of the films. TPA-DPP film exhibited weak diffraction peaks at 2θ of 5.74° and 5.30° , corresponding to the d -spacings of 15.38 \AA and 16.65 \AA . It was clear that TPA-DPP-MDN exhibited a second order diffraction peak at 11.82° (a d -spacing of 7.48 \AA). Furthermore, two additional sets of reflections were at 2θ of 17.52° and 20.75° with d -spacings of 5.06 \AA , and 4.28 \AA . According to the XRD information, the TPA-DPP-MDN film possessed higher degree of crystallinity than the TPA-DPP film.

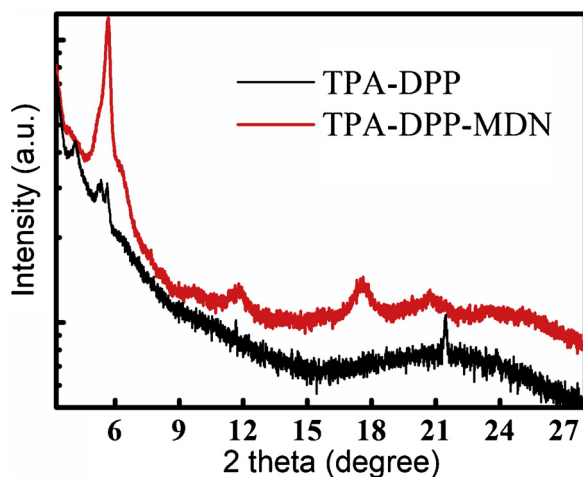


Fig. 3. XRD patterns of the pristine TPA-DPP-MDN and TPA-DPP thin films.

3.4. Optical properties

The UV–vis absorption spectra of two SMDs in solution and solid thin films were displayed in Fig. 4, and the related data were summarized in Table 1. In comparison with TPA-DPP, TPA-DPP-MDN both in solution and in film (Fig S14) are greatly broadened and red-shifted, respectively. Moreover, the TPA-DPP-MDN exhibits a higher molar extinction coefficient (ϵ) than that of TPA-DPP (Fig. S14). The TPA-DPP showed main absorption peak at 590 nm with the absorption edge (λ_{onset}) located at 646 nm in chloroform solution. The absorption peak and edge of TPA-DPP-MDN in chloroform solution were red shifted of 51 nm and 99 nm relative to these of TPA-DPP. As shown in Table 1 and

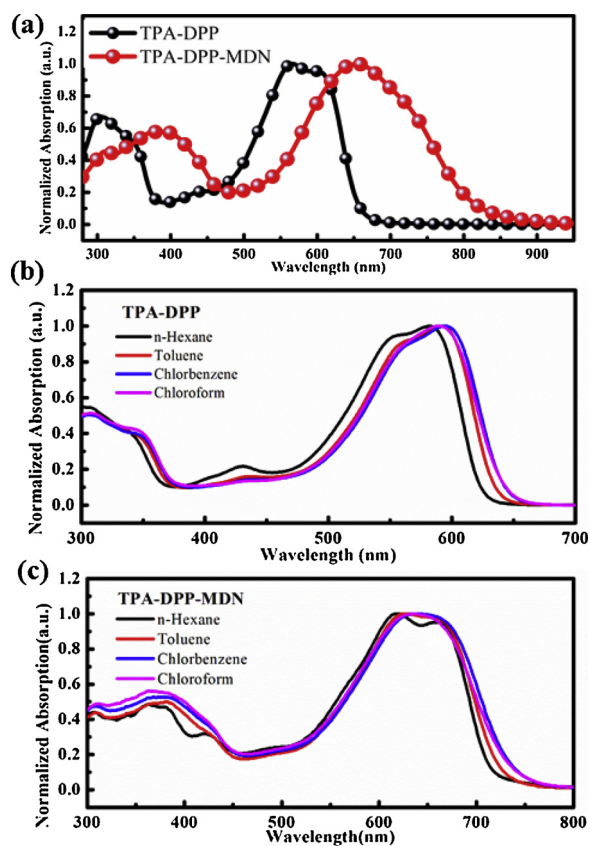


Fig. 4. (a) Normalized UV–vis absorption spectra of TPA-DPP and TPA-DPP-MDN in thin film; Normalized UV–vis absorption spectra of TPA-DPP-MDN (b) and TPA-DPP (c) in different solvent.

Table 1

UV–vis absorption data of TPA-DPP and TPA-DPP-MDN in different solvent.

Solvents	n-Hexane	Toluene	Chlorobenzene	Chloroform
TPA-DPP λ_{onset} (nm)	624	635	642	646
TPA-DPP-MDN λ_{onset} (nm)	715	725	739	745

Fig. 4. (b) and (c), with the increase of the solvent polarity gradually from hexane to chloroform, TPA-DPP exhibited a little red-shifted by 22 nm from peak of 624 nm (in n-hexane) to 646 nm (in chloroform). In contrast, the absorption behavior of TPA-DPP-MDN with increase of the solvent polarity showed red-shifted of 30 nm with broader shape. The difference of the absorption bands registered could be ascribed to the different structures of the push-pull system in which the auxiliary electron-withdrawing unit (MDN) extended the conjugation length in the backbone facilitated the intramolecular electron transfer, and thus modulated the response of the light-harvesting range. Fig. 4. (a) showed the UV–vis absorption spectra of two SMDs in thin film. The absorption peak and band edge of TPA-DPP film were at 600 nm and 675 nm, which was red-shifted by 10 nm and 29 nm with respect to these in chloroform. In comparison with the spectra of TPA-DPP-MDN in chloroform, its spectra were greatly broadened and red-shifted with absorption peak and band edge at 657 nm and 818 nm in film. Obviously, the absorption band edge of TPA-DPP-MDN film was red-shifted by 73 nm with regard to its absorption in chloroform, which was consistent with the XRD information indicating the strong intermolecular interaction in the solid-state. The optical E_g of TPA-DPP and TPA-DPP-MDN was 1.89 eV and 1.52 eV, respectively, corresponding to their absorption onset in film. Compared with D-A structure, the D-A-A system showed an extended the spectral region with a low energy gap. The fluorescence spectra of TPA-DPP (a) and TPA-DPP-MDN (b) in different solvents were shown in Fig. 5. The Photoluminescence (PL) behaviors of TPA-DPP and TPA-DPP-MDN were compared to emphasize the Push-Pull character. TPA-DPP exhibited a little red-shift of 24 nm with increase of the solvent polarity gradually from Hexane to Chlorobenzene (CB). It was noted that all of the PL spectra of TPA-DPP showed the similar shape in solutions. Moreover, full width at half maximum (FWHM) of TPA-DPP seemed to be independent with solvent polarity. However, compared with these of TPA-DPP, the fluorescent spectra of TPA-DPP-MDN showed the larger red-shifted of 35 nm, broader shape with increase of the solvent polarity, a FWHM of 129 nm in CB. This change was consistent with a variety of the excited state characteristics, which indicated that D-A-A compound presented the remarkable push-pull effect.

3.5. Electrochemical properties

The energy levels of the SDMs were determined by cyclic voltammetry (CV). The CV curves were shown in Fig. 6 (a), and the results of the electrochemical measurements were summarized in Table 2. The CV curves were determined by the reference electrode (Ag/Ag^+), which was referenced to ferrocene/ferrocenium (Fc/Fc^+) redox couple (4.8 eV below the vacuum level) [30]. TPA-DPP exhibited the onset reduction potential at -1.14 V. It was noted that TPA-DPP-MDN shown two onset reduction at -1.05 and -1.45 V, which were ascribed to the reduction of the DPP and the MDN group, respectively. The onset oxidation potentials (E_{OX}) of TPA-DPP and TPA-DPP-MDN were around 0.43 V and 0.48 V. The HOMO and LUMO energy levels were calculated by empirical formula [31] $E_{\text{HOMO}} = -(E_{\text{OX}} + 4.70)$ (eV) and $E_{\text{LUMO}} = -(E_{\text{Red}} + 4.70)$ (eV), -5.13 and -3.56 eV for TPA-DPP, -5.18 and -3.65 eV for TPA-DPP-MDN, respectively. As shown in the energy levels of the SDMs and acceptor (Fig. 5. (b)). It was clear that the HOMO energy levels decreased slightly in the order: D-A and D-A-A. The LUMO energy level of D-A-A system was 0.09 eV lower than the level of D-A system. The low-lying HOMO level of TPA-DPP-MDN would ensure a relatively

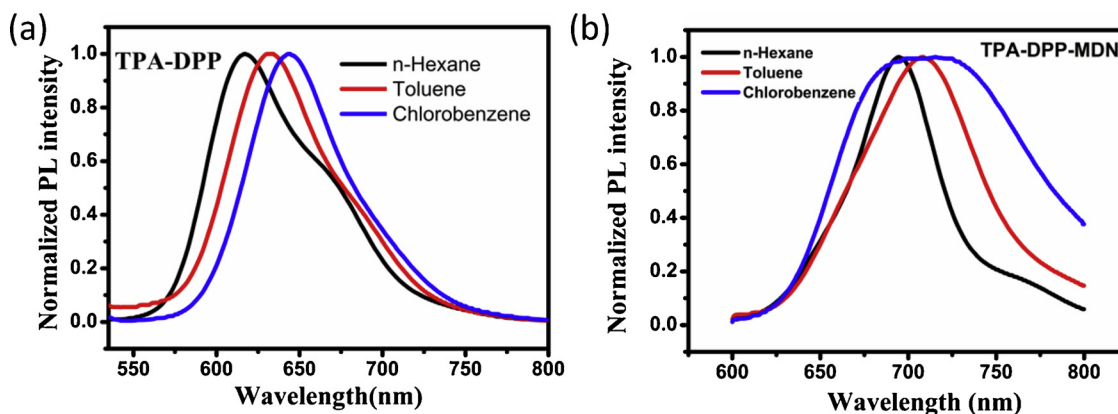


Fig. 5. Normalized fluorescence spectra of TPA-DPP (a) and TPA-DPP-MDN (b) in different solvents.

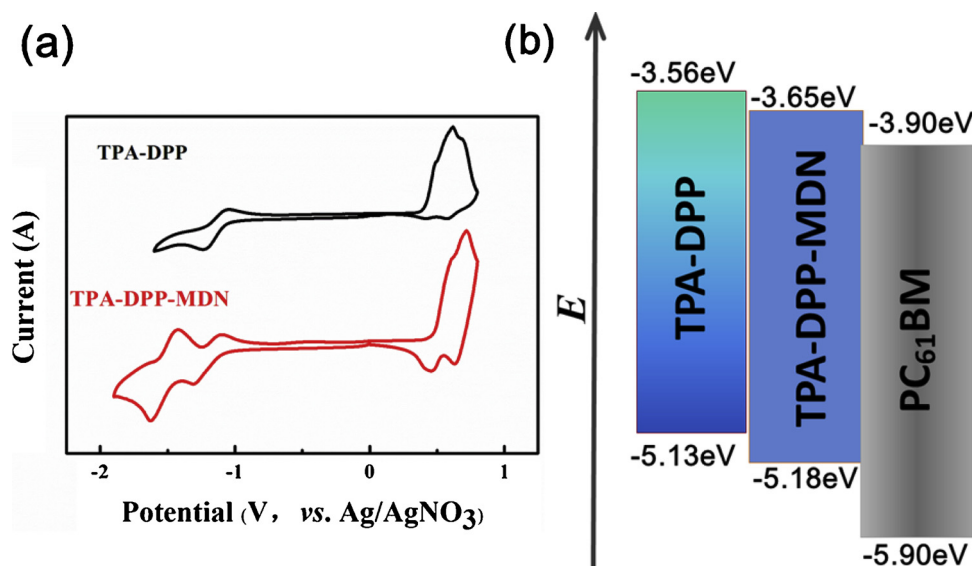


Fig. 6. (a) CV curves of compound TPA-DPP and TPA-DPP-MDN in 0.1 mol·L⁻¹ Bu₄NPF₆ acetonitrile solution at a sweep rate of 100 mV·s⁻¹; (b) Energy levels of the components.

Table 2
Optical and electrochemical characteristics of the TPA-DPP and TPA-DPP-MDN.

Compound	$\lambda_{\text{onset}}^{\text{film}}$ (nm)	$E_g^{\text{opt}^1}$ (eV)	E_{oxonset} (V)	E_{redonset} (V)	ECV g (eV)	ECV HOMO ² (eV)	ECV LUMO ³ (eV)
TPA-DPP	657	1.89	0.43	-1.14	1.57	-5.13	-3.56
TPA-DPP-MDN	818	1.52	0.48	-1.05	1.53	-5.18	-3.65

¹ Calculated from the onset of the film absorption ($E_g = 1240/\lambda_{\text{onset}}$).

² Calculated from oxidation potential of the copolymer ($\text{ECV HOMO} = -(E_{\text{ox}} + 4.70)$ (eV)).

³ Calculated from reduction potential of the copolymer ($\text{ECV LUMO} = -(E_{\text{red}} + 4.70)$ (eV)).

higher V_{OC} than that of TPA-DPP. In addition, compared with the counterpart TPA-DPP, TPA-DPP-MDN exhibited higher oxidation peak potential. The electrochemical data were in agreement with the computational results which clearly indicate that the HOMO level of the TPA-DPP-MDN was lower than that of the TPA-DPP attributed to the electron-withdrawing effect of the auxiliary unit. In fact, the MDN unit afforded also a decrease of the LUMO level, which was lowered by a larger amount than the HOMO level, resulting in a decrease of the energy gap of D-A-A compound.

3.6. Photovoltaic properties of two molecules

The PV properties of the SMDs were examined by fabricating bulk heterojunction (BHJ) OSCs with device architecture of ITO/PFN/

Blends/MoO₃/Ag. The active layers containing various D/A ratios have been fabricated by spin-casting a solution of SMDs and [6,6]-phenyl-C₆₁-butyric acid methyl ester (PC₆₁BM) mixtures dissolved in chloroform. The OSCs were tested under AM 1.5 G (Air mass 1.5 global, 100 mW·cm⁻²). The current density-voltage (J - V) characteristics were shown in Fig. 7. (a), and detailed parameters of the devices were listed in Table 3. The OSC based on TPA-DPP-MDN/PC₆₁BM (w:w, 1:3) blend showed the power conversion efficiency (PCE) of 1.12%, with a V_{OC} of 0.74 V, a J_{SC} of 4.61 mA·cm⁻², and a fill factor (FF) of 32.84%. The OSCs based on TPA-DPP/PC₆₁BM (w:w, 1:3) blend showed the PCE of 0.35%, with a V_{OC} of 0.65 V, a J_{SC} of 1.80 mA·cm⁻², and a FF of 29.71%. Evidently, the high V_{OC} of D-A-A system based device was originated from the low-lying HOMO level of TPA-DPP-MDN, due to the electron-withdrawing effect of the auxiliary unit. The IPCE curves of the devices

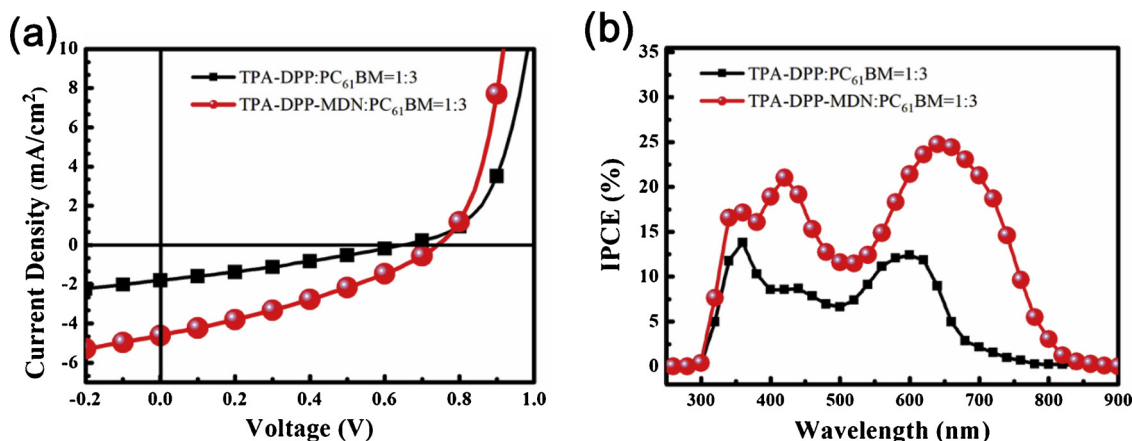


Fig. 7. (a) J - V curves of BHJ devices with a configuration of ITO/PFN/Blends/MoO₃/Ag under an illumination of AM 1.5 G at 100 mW·cm⁻²; (b) The IPCE curves of the OSCs based on the SMDs:PC₆₁BM.

Table 3

Photovoltaic parameters of the OSCs based on the SMDs and PC₆₁BM.

Active layer	w:w	V _{OC} (v)	J _{SC} (mA·cm ⁻²)	FF (%)	PCE (%)
TPA-DPP-MDN/PC ₆₁ BM	1:3	0.74	4.61	32.84	1.12
TPA-TDPP/PC ₆₁ BM	1:3	0.65	1.80	29.71	0.35

based on the SMDs/PC₆₁BM blends with the weight ratio of 1:3 were shown in Fig. 7. (b). The device of TPA-DPP/PC₆₁BM exhibited photoresponse in the range of 300–700 nm. Remarkably, the IPCE curves showed the range of 300–800 nm for TPA-DPP-MDN/PC₆₁BM device, which extended by 100 nm compared with TPA-DPP/PC₆₁BM device. The integrated J_{SC} values for the two OSCs were 1.80 mA·cm⁻² of TPA-DPP/PC₆₁BM and 4.61 mA·cm⁻² of TPA-DPP-MDN/PC₆₁BM, which were close to the J_{SC} values obtained from J - V measurements. And thus, an important factor that contributed to the enhanced J_{SC} in TPA-DPP-MDN was the photon absorption over the near-IR range due to the reduced energy bandgap. The significantly improved performance in D-A-A system based device was mainly attributed to higher J_{SC} and V_{OC} due to the reduced energy bandgap and the low-lying HOMO level.

4. Conclusion

In conclusion, two asymmetric push-pull molecules with D-A and D-A-A architectures (TPA-DPP and TPA-DPP-MDN) have been synthesized and applied in the investigation of solution-processes BHJ OSCs. TPA-DPP-MDN has a better thermal stability and possessed higher degree of crystallinity in film with respect to these of TPA-DPP. Furthermore, the auxiliary electron-withdrawing unit enabled D-A-A SMD to exhibit a narrow E_g and a low-lying HOMO level, which resulted in a high J_{SC} and V_{OC}, and a significantly improved performance of the BHJ OSCs. The results gave an important guide for developing novel asymmetrical D-A-A system SMDs.

Acknowledgements

The authors are deeply grateful to National Natural Science Foundation of China (No: 61404067, 51602139), the Natural Science Foundation of Gansu Province (no.18JR3RA108) and Lanzhou Jiaotong University-Tianjin University Joint Innovation Fund Project Funding (2019056). We also express our gratitude to Instrument Analysis Center of Lanzhou Jiaotong University for related testing support.

Appendix A. Supplementary data

Supplementary material related to this article can be found, in the

online version, at doi:<https://doi.org/10.1016/j.jphotochem.2019.112139>.

References

- [1] Y. Liu, C.-C. Chen, Z. Hong, J. Gao, Y. (Michael) Yang, H. Zhou, L. Dou, G. Li, Y. Yang, Sci. Rep. Ist. Super. Sanita 3 (2013) 3356.
- [2] B. Kan, M. Li, Q. Zhang, F. Liu, X. Wan, Y. Wang, W. Ni, G. Long, X. Yang, H. Feng, Y. Zuo, M. Zhang, F. Huang, Y. Cao, T.P. Russell, Y. Chen, J. Am. Chem. Soc. 137 (2015) 3886–3893.
- [3] Q. Zhang, B. Kan, F. Liu, G. Long, X. Wan, X. Chen, Y. Zuo, W. Ni, H. Zhang, M. Li, Z. Hu, F. Huang, Y. Cao, Z. Liang, M. Zhang, T.P. Russell, Y. Chen, Nat. Photonics 9 (2015) 35–41.
- [4] W. Li, D. Wang, S. Wang, W. Ma, S. Hedström, D.I. James, X. Xu, P. Persson, S. Fabiano, M. Berggren, O. Inganäs, F. Huang, E. Wang, ACS Appl. Mater. Interfaces 7 (2015) 27106–27114.
- [5] S.-Y. Shiao, C.-H. Chang, W.-J. Chen, H.-J. Wang, R.-J. Jeng, R.-H. Lee, Dye. Pigment. 115 (2015) 35–49.
- [6] A. Mishra, P. Bäuerle, Angew. Chem. Int. Ed. 51 (2012) 2020–2067.
- [7] Y. Lin, Y. Li, X. Zhan, Chem. Soc. Rev. 41 (2012) 4245–4272.
- [8] Y. Chen, X. Wan, G. Long, Acc. Chem. Res. 46 (2013) 2645–2655.
- [9] L. Yuan, K. Lu, B. Xia, J. Zhang, Z. Wang, Z. Wang, D. Deng, J. Fang, L. Zhu, Z. Wei, Adv. Mater. 28 (2016) 5980–5985.
- [10] J.E. Coughlin, Z.B. Henson, G.C. Welch, G.C. Bazan, Acc. Chem. Res. 47 (2014) 257–270.
- [11] A. Mishra, D. Popovic, A. Vogt, H. Kast, T. Leitner, K. Walzer, M. Pfeiffer, E. Mena-Osteritz, P. Bäuerle, Adv. Mater. 26 (2014) 7217–7223.
- [12] X. Liu, Y. Sun, B.B.Y. Hsu, A. Lorbach, L. Qi, A.J. Heeger, G.C. Bazan, J. Am. Chem. Soc. 136 (2014) 5697–5708.
- [13] J.-Q. Xu, W. Liu, S.-Y. Liu, J. Ling, J. Mai, X. Lu, C.-Z. Li, A.K.-Y. Jen, H. Chen. Sci. China Chem. 60 (2017) 561–569.
- [14] R. Fitzner, E. Mena-Osteritz, K. Walzer, M. Pfeiffer, P. Bäuerle, Adv. Funct. Mater. 25 (2015) 1845–1856.
- [15] V. Jeux, O. Segut, D. Demeter, T. Rousseau, M. Allain, C. Dalinot, L. Sanguinet, P. Leriche, J. Roncali, Dye. Pigment. 113 (2015) 402–408.
- [16] O. Vybornyi, Y. Jiang, F. Baert, D. Demeter, J. Roncali, P. Blanchard, C. Cabanetos, Dye. Pigment. 115 (2015) 17–22.
- [17] Q. Shi, P. Cheng, Y. Li, X. Zhan, Adv. Energy Mater. 2 (2012) 63–67.
- [18] S. Paek, N. Cho, Song K, M.-J. Jun, J.K. Lee, J. Ko, J. Phys. Chem. C 116 (2012) 23205–23213.
- [19] F. Baert, C. Cabanetos, M. Allain, V. Silvestre, P. Leriche, P. Blanchard, Org. Lett. 18 (2016) 1582–1585.
- [20] Y. Jiang, C. Cabanetos, M. Allain, S. Jungsttiwong, J. Roncali, Org. Electron. 37 (2016) 294–304.
- [21] J.K. Lee, J. Kim, H. Choi, K. Lim, K. Song, J. Ko, Tetrahedron (2014) 1–6.
- [22] L.-Y. Lin, Y.-H. Chen, Z.-Y. Huang, H.-W. Lin, S.-H. Chou, F. Lin, C.-W. Chen, Y.-H. Liu, K.-T. Wong, J. Am. Chem. Soc. 133 (2011) 15822–15825.
- [23] Y.-H. Chen, L.-Y. Lin, C.-W. Lu, F. Lin, Z.-Y. Huang, H.-W. Lin, P.-H. Wang, Y.-H. Liu, K.-T. Wong, J. Wen, D.J. Miller, S.B. Darling, J. Am. Chem. Soc. 134 (2012) 13616–13623.
- [24] S.-W. Chiu, L.-Y. Lin, H.-W. Lin, Y.-H. Chen, Z.-Y. Huang, Y.-T. Lin, F. Lin, Y.-H. Liub, K.-T. Wong, Chem. Commun. (Camb.) 48 (2012) 1857–1859.
- [25] H. Gao, Y. Li, L. Wang, C. Ji, Y. Wang, W. Tian, X. Yang, L. Yin, Chem. Commun. (Camb.) 50 (2014) 10251–10254.
- [26] D. Wang, X. Zhang, W. Ding, X. Zhao, Z. Geng, Comput. Theor. Chem. 1029 (2014) 68–78.
- [27] Y. Cui, P. Li, C. Song, H. Zhang, J. Phys. Chem. C 120 (2016) 28939–28950.
- [28] J. Liu, Y. Sun, P. Moonsin, M. Kuik, C.M. Proctor, J. Lin, B.B. Hsu, V. Promarak, A.J. Heeger, T.-Q. Nguyen, Adv. Mater. 25 (2013) 5898–5903.
- [29] J. Frisch, M.G. Trucks, H. Schlegel, G. Scuseria, M. Robb, J. Cheeseman, et al., Gaussian 09, Revision A.01, Gaussian, Inc., Wallingford CT, 2009.
- [30] J. Pommerene, H. Vestweber, W. Guss, R.F. Muhr, H. Bässler, M. Porsch, J. Daub, Adv. Mater. 7 (1995) 551–554.
- [31] W. Gao, T. Liu, M. Hao, K. Wu, C. Zhang, Y. Sun, C. Yang, Chem. Sci. 7 (2016) 6167–6175.